Available online at www.sciencedirect.com
ScienceDirect
Applied Catalysis B: Environmental 80 (2008) 32–41
APPLIED CATALYSIS B: ENVIRONMENTAL
www.elsevier.com/locate/apcatb

Synthesis, characterization and catalytic activity of easily recyclable zinc oxide nanobundles

M. Muruganandham, J.J. Wu *

Department of Environmental Engineering and Science, Feng Chia University, Taichung 407, Taiwan

Received 13 July 2007; received in revised form 16 October 2007; accepted 13 November 2007
Available online 19 November 2007

Abstract

A new self-assembly of ZnO nanobundle has been successfully synthesized in this research by thermal decomposition of zinc oxalate at atmospheric pressure without using any catalyst or solvent at moderate temperature. The XRD analysis showed that the synthesized nanobundles are hexagonal wurtzite-type pure polycrystalline zinc oxide and high resolution transmission electron microscope (HR-TEM) analysis showed that the synthesized nanoparticles size was 0–30 nm, and increases up to 10–70 nm during the bundle formation. To test the catalytic activity of ZnO nanobundles in catalytic ozonation process, 2-ethoxy ethyl acetate (2-EEA) was used as the model organic pollutant. The results show that the presence of ZnO nanobundles in ozonation process could further enhance 39.7% of 2-EEA decomposition and 9.5% of TOC removal. Increase the catalyst loading from 0.2 to 2 g/l would increases the removal rate appreciably. Further increase in the catalyst loading could not enhance the removal rate significantly. Since the direct reaction rate constant (k_D) was found to be 0.675 $M^{-1} S^{-1}$, implying that ozone is not a potential oxidizing agent for 2-EEA direct oxidation, catalytic ozonation is thus necessitated to accelerate the decomposition of 2-EEA by hydroxyl radicals produced in the catalytic ozonation process. AAS analysis showed that zinc ion was not leached from the catalysts in all experiments. The catalytic reusability was investigated up to four successive cycles and found that the catalytic efficiency was not decreased appreciably. The catalytic recyclability of nanobundles are investigated and compared with other nanoparticles such as ZnO and TiO_2-P25, and found that nanobundles are easily recyclable when compared to the above said nanoparticles. It is concluded that the nanobundles are effective and easily recyclable in catalytic ozonation process.

Keywords: Nanobundles; ZnO; Catalytic ozonation; Ozone; 2-EEA

1. Introduction

Semiconductor nanocrystals have attracted a great attention from researchers on their wide range of applications. One of the important goals of material scientists has been tailoring the structure to obtain particular morphologies for the design and development of new materials suitable for more advanced applications. The synthesis and understanding of the growth of new ZnO nanostructures and their applications are at the leading edge of today's research in nanotechnology. Currently, many interesting ZnO nanostructures, including nanobelts [1], nanorods [2], nanowires [3], nanosheets and nanonails [4], nanopencils [5], nanobridges [6], have been proposed by using various preparation approaches. Thus, it is necessary to prepare these ZnO nanomaterials by simple routes which do not involve complex procedures, sophisticated equipment, or rigid experimental conditions.

Self-assembly of colloidal particle into larger aggregates is not principally new and is well known phenomenon in colloid chemistry. Penn and Banfield [7–9] reported oriented attachment of crystal growth concept and found that the aggregates of bulk crystals are formed either perfectly aligned crystalline lattice planes or dislocations at the contact areas between the adjacent particles of TiO_2 anatase and iron oxide nanoparticles under hydrothermal conditions. Self-assembly of ZnO nanodots to nanorods by oriented attachment was reported by Pacholski et al. [10] under refluxed conditions. Although, thermal decomposition of zinc oxalate to zinc oxide is a known process and well documented in the literature [11–13], the formation of ZnO nanobundles from zinc oxalate thermal decomposition was not reported in the literature. Recently, homocentric ZnO nanobundles with pyramid like and hexagonal prism shapes have been

* Corresponding author. Tel.: +886 4 24517250x5206; fax: +886 4 24517686.
E-mail address: jjwu@fcu.edu.tw (J.J. Wu).

0926-3373/$ – see front matter
doi:10.1016/j.apcatb.2007.11.006

reported [14]. For the first time, we report the fabrication of chain like, high quality polycrystalline hexagonal wurtzite ZnO nanobundles and its catalytic activity.

Ozone is an environment friendly oxidant since it decomposes into oxygen without producing self-derived byproducts in the oxidation reaction. Unfortunately, some oxidation products are refractory to further oxidative conversion by means of ozone, thus preventing a complete abatement of TOC. However, the high energy cost for its generation might limit many practical applications of direct ozonation. Therefore, it is highly recommended to conduct very effective methods for their removal from waters by degrading them, either to less harmful intermediates or to complete mineralization. Heterogeneous catalytic ozonation is a novel type of advanced oxidation that combines ozone with the adsorptive and oxidative properties of solid phase metal oxide catalysts to achieve mineralization of target organics at room temperature. Some studies on the heterogeneous catalytic ozonation using alumina, manganese oxide, titanium dioxide, and activated carbon substances have been previously reported [15–18]. Most nanocrystalline catalysts substantially exhibit high catalytic properties in catalytic ozonation reactions using suspensions of powdered materials. However, the separation of these nanocrystals from the treated water is very difficult and energy-consumptive. Thus, intensive research has been focused on the preparation of active immobilized catalysts for water treatment. Although, ZnO catalyzed ozone decomposition as well as organic pollutant degradation was reported in the literature [19,20], the ZnO nanobundles catalyzed decomposition has not been reported yet.

In the present study, 2-ethoxy ethyl acetate (2-EEA) was chosen as a model organic pollutant. To the best of our knowledge, no reports are available for detailed 2-EEA decomposition and mineralization using catalytic ozonation process and ZnO bundles as a catalyst. 2-EEA is frequently used in automobile lacquers to retard evaporation and impart high gloss. In addition, it is used as a solvent for oils, resins, and nitrocellulose. It is also used in wood stains, leather and cosmetic ingredients and in the semiconductor industry as a component of cleaning solution (photoresist stripper). When released into the soil, 2-EEA is expected to leach into groundwater and due to its high boiling point it is not evaporated significantly. Therefore, the aim of this study was to investigate the decomposition efficiency of 2-EEA using ZnO nanobundles in catalytic ozonation process.

2. Experimental procedure

2.1. Chemicals

2-EEA (99.8%) TEDIA chemicals, HPLC grade acetonitrile, and *t*-butanol (99%) were purchased from Merck Co., Taiwan. Oxalic acid (anhydrous) (99%), ZnO nanoparticle and zinc nitrate hexa hydrate (99%) were obtained from SHOWA Chemical Co., Japan. Indigo dye from ACROS organics was of analytical grade and used without further purification. The surface properties of synthesized ZnO nanobundles are presented in Table 1. For all experimental work, deionized water Milli q-Plus, resistance = 18.2 M Ω, was used. The pH of aqueous solution was maintained at 3.0 ± 0.1 throughout the experiments and adjusted by using 70% $HClO_4$.

2.2. Catalytic ozonation experiments

Ozone was generated from dried pure oxygen by corona discharge using an ozone generator (Ozonair RXO-5), which can produce 6% ozone concentration (w/w) in the oxygen enriched gas stream. To better maintain the performance of the ozonation system, the oxygen was dried using a molecular sieve before being entered into the ozone generator. A 0.5–l semibatch reactor, which was made of glass with the dimensions of 9 cm diameter and 15 cm tall, was used to facilitate the operation of all catalytic oxidation processes (Fig. 1). Ozone was introduced through a porous fritted diffuser that can produce fairly fine bubbles with diameter less than 1 mm, which had been determined using a camera with close-up lens and image analysis software Matrox Inspector 2.0 [21]. The gas flow rate was regulated by a mass flow controller (Brooks 5850E). The gaseous ozone concentration in the inlet and outlet stream were determined and monitored spectrophotometrically by the absorbance of ozone measured in a 2-mm flow-through quartz cuvette at the wavelength 254 nm. An extinction coefficient of 3000 M^{-1} cm^{-1} was used to convert absorbance into concentration units [21]. Ozone applied dosage is typically defined as the product of gas flow rate, ozone concentration, and ozonation period, divided by the reactor volume. A 500 ml solution containing appropriate concentration of 2-EEA and catalyst was placed in a reactor and in order to make homogeneous slurries, the solution was magnetically stirred at the speed of 900 rpm. After few minutes of stirring, ozone was introduced into the reactor. All experiments were operated at 25 °C using a water jacket around the reactor.

2.3. 2-Ethoxy ethyl acetate analysis

Samples were withdrawn from the reactor at desired time intervals in the course of the experiments. The residual dissolved ozone in the samples was immediately removed by flushing with nitrogen gas (99.99%). The catalyst was centrifuged and filtrated through Whatman glass micro fiber filter paper (47 mm diameter size and 0.1 μm pore size) in order to remove the catalyst. The dissolved ozone concentration was measured using indigo method [22]. 2-EEA concentration was analyzed using auto sampler HPLC (Spectra System-1000,

Table 1
Surface properties of ZnO nanobundles

Properties	Values
BET surface area	11.9 m^2/g
Total pore volume (single point)	0.37 cm^2/g
Average pore diameter (4 V/A by BET)	125.9 A
BJH average pore diameter (4 V/A)	419.6 A
Average pore hydraulic radius (V/A)	5.84 A

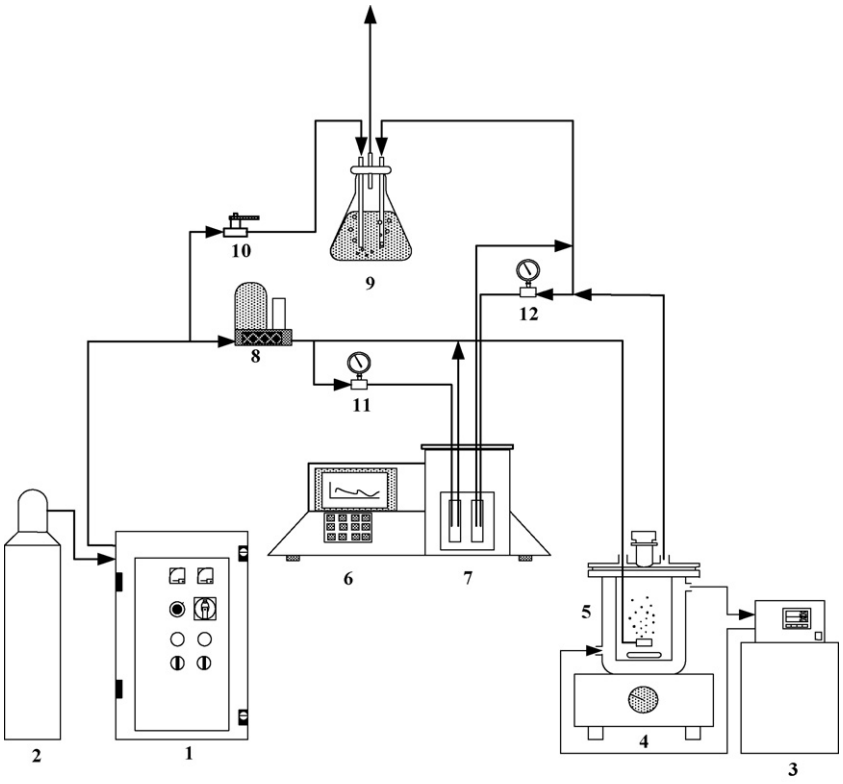

Fig. 1. System setup for ozonation and catalytic ozonation experiments.

Chrom Quest) equipped with an ultra aqua C_{18} column (5 μm, 250 mm × 4.6 mm) employing UV detection at wavelength of 214 nm. The mobile phase consisted of water containing acetonitrile with a ratio of 50:50 and the flow rate was controlled at 1.0 ml/min. The retention time of 2-EEA is 4.9 min and the standard deviation of these retention times was lower than 0.1 min. The detection limit for 2-EEA analysis using HPLC is 3 mg/l. TOC concentrations were measured using Rosemount Dohrmann TOC analyzer.

2.4. Preparation of zinc oxalate dihydrate

Aqueous solutions of equal volume of 0.4 M zinc nitrate hexahydrate and of 0.6 M unhydrous oxalic acid in deionized water (Milli q-Plus, resistance = 18.2 M Ω) were brought to their boiling points and the former was added rapidly to the latter; the mixture was stirred often as it cooled to room temperature. The precipitate is rather fine and uniform in dimension. The crystals were washed several times with distilled water, air-dried for over night, and dried 100 °C for 3 h. The sample was kept for further analysis in polyethylene cover.

2.5. Zinc oxalate dihydrate decomposition

About 500 mg of zinc oxalate dihydrate was taken in a porcelain dish and kept inside the muffle furnace. The furnace was heated at the rate of 20 °C/min to reach the decomposition temperature (400 °C). After 12 h, the furnace was allowed to cool down to room temperature. The nanobundle was collected and used for further analysis.

2.6. Analytical methods

Total zinc ion (Zn^{2+}) was measured using Hitachi AA-464 flame atomic absorption spectrometry (AAS) with Hollow cathode lamp. The surface area, pore size, and pore volume of the ZnO nanobundles were measured by nitrogen adsorption at 77.35 K using an accelerated surface area and porosity apparatus (ASAP 2010, Micromeritics). Prior to analysis,

1–2 g of powder was degassed at 473 K and 200 mm Hg for 2 h. The X-ray diffraction (XRD) patterns were recorded using a MAX SCIENCE MXP3 diffractometer and Cu Kα radiation and 2θ scanned angle from 10° to 80° at the scanning rate of 2° per min. High resolution transmission electron microscope (HR-TEM) images recorded using JEOL JEML-2010 high resolution transmission electron microscope. Samples for HR-TEM were prepared by ultrasonically dispersing the ZnO into absolute ethanol, then placing a drop of this suspension onto a copper grid and then drying in air. The working voltage of TEM was 200 kV. The morphology of the catalyst was examined using a Hitachi S-4800 cold field emission scanning electron microscope (FESEM) equipped with HORIBA EMAX 400 energy dispersive X-ray microanalysis (EDX) systems. Prior to FESEM measurements, the samples were mounted on carbon platform. The plate containing the sample was placed in the scanning electron microscope for the analysis with desired magnifications. The percentage of degradation of 2-EEA and TOC of sample was calculated from the following expressions

$$\text{Degradation}(\%) = \frac{C_{(2\text{EEA})0} - C_{(2\text{EEA})}}{C_{(2\text{EEA})0}} \times 100$$

$$\text{TOC}(\%) = \frac{C_{(\text{TOC})0} - C_{(\text{TOC})t}}{C_{(\text{TOC})0}} \times 100$$

where $C_{(2\text{-EEA})0}$ and $C_{(\text{TOC})0}$ are initial concentration of 2-EEA, TOC and $C_{(2\text{-EEA})t}$ and $C_{(\text{TOC})t}$ concentration after time t, respectively.

3. Results and discussion

3.1. Characterizations of zinc oxide nanobundles

The as-synthesized zinc oxalate dihydrate was characterized using XRD, differential scanning calorimetry (DSC), thermo gravimetric analysis (TGA) and FESEM. The XRD peaks (Fig. 2) were consistent with α-$C_2O_4Zn{\cdot}2H_2O$ [JCPDS Card No. 25–1029]. DSC–TGA results as shown in Fig. 3, also confirmed the formation of pure zinc oxalate dihydrate and the decomposition results are well matched with zinc oxalate dihydrate decomposition reported in the literature [13,23]. FESEM analysis showed that the zinc oxalate dihydrate display no defined size or shape as shown in Fig. 4a.

The thermal decomposition of zinc oxalate dihydrate in air has been studied and analyzed using XRD and FESEM techniques. XRD results indicated that the as-synthesized α-$C_2O_4Zn{\cdot}2H_2O$ decomposed completely in 15 min. No other impurity peaks appear in X-ray diffraction peak, which indicates the formation of pure ZnO. All the marked diffraction peaks of ZnO in Fig. 2 can coincidently be indexed by the known hexagonal standard ZnO (JCPDS Card No. 89-0511), the crystallographic phase of these ZnO nanobundles belongs to the wurtzite-type ZnO (SG:*P*63*mc*). Characteristic peaks of ZnO at 31.68, 34.36, 36.18 and 56.56, corresponded to [1 0 0], [0 0 2], [1 0 1] and [1 1 0] diffraction peaks of wurtzite ZnO, indicate that ZnO shell possess a hexagonal crystal structure. The relative high intensity of the [1 0 1] peak is indicative of

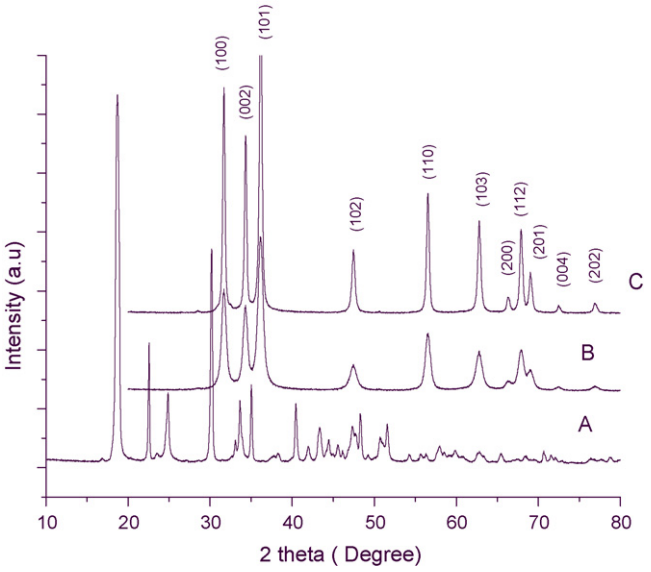

Fig. 2. XRD analysis of zinc oxalate dihydrate and zinc oxide: (A) zinc oxalate dihydrate, (B) zinc oxalate dihydrate decomposition after 15 min at 400 °C, and (C) zinc oxalate dihydrate decomposition after 12 h at 400 °C.

anisotropic growth and implies a preferred orientation of the crystallites. By increasing the decomposition time (15 min to 12 h at 400 °C), ZnO peaks become sharper, which indicates that ZnO is well crystallized and the particle size was increased.

3.2. Nanobundles formation

In our experiment, it was found that the as-synthesized ZnO nanobundles are of about 100% reproducibility from run to run. Zinc oxalate is completely decomposed into ZnO in 15 min at 400 °C and forms a corn like ZnO nanoparticle chain. It seems that the formed nanoparticle chains are arranged irregularly with different length and all the nanoparticles are not completely coalescent in the chains. If the heating time is further extended, these nanoparticles are coalescing together

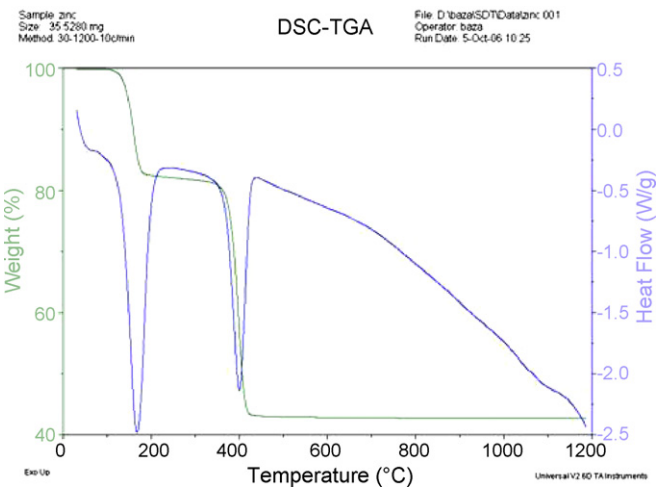

Fig. 3. DSC–TGA analysis of zinc oxalate dihydrate.

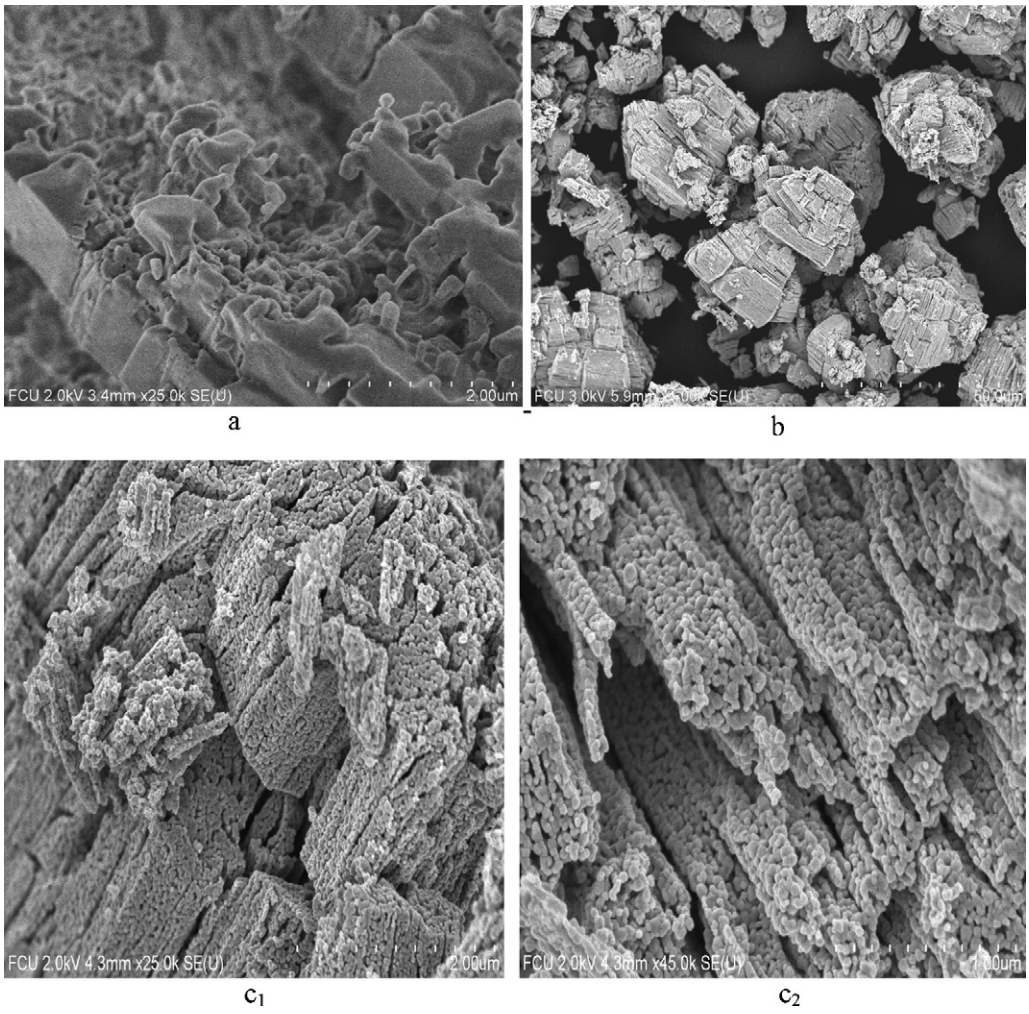

Fig. 4. FESEM pictures of (a) zinc oxalate dihydrate [×25k], (b) ZnO nanobundles at low magnification [×1k], and (c) ZnO nanobundles at high magnification c_1 = [×25k] and c_2 = [×45k].

form an ordered chain due to the thermal effect, while the same time adjacent chains are coalescent to form small nanobundles. After 12 h, these small nano chain bundles are fused together to form big chain bundles of various sizes. The particle size of ZnO nanoparticle has been analyzed in HR-TEM and shown in Fig. 5. It can be seen that after 20 min of heating at 400 °C, the ZnO particle size was in the range from 0 to 30 nm with an average particle size of 18.4 nm. However, after 12 h of heating these particles size was increased from 10 to 70 nm. HR-TEM lattice fringes image (Fig. 6) indicated that these nanoparticles coalesce by imperfect-oriented attachment (IOA). Clear lattice fringes also demonstrate that the nanoparticles are highly crystallized. Selected area electron diffraction (SAED) pattern reveals that the as-synthesized ZnO bundles are polycrystalline nature as shown in Fig. 7.

3.3. Mechanism of nanobundle formation

Various self-assembly processes based on different driving mechanisms have been reported [10,24–26]. Among which, 'perfect/imperfect oriented attachment' has attracted much attention recently as an effective mechanism for fabricating novel complex nanostructures [27–29]. This mechanism is based on self-assembly of primary particles followed by spontaneous adjustment and lattice fusion of the adjacent crystallographic planes, in an ideal case of which the particles are free to move in, for example, liquid or gas environment [7]. Although, many reports are available for ZnO preparation from zinc oxalate decomposition at various experimental conditions, no nanobundle formation has been reported in the literature. According to our studies, it is interesting to note that the decomposition temperature and time are the most important parameters for nanobundle formation. HR-TEM lattice fringes showed that the nanoparticles are coalescent by imperfect-oriented attachment. ZnO has a wurtzite structure with a hexagonal unit cell owing to three fastest growth directions, $(0\,0\,0\,1 > 0\,1\,\bar{1}\,0 > 2\,\bar{1}\,\bar{1}\,0)$ as well as $\pm(0\,0\,0\,1)$ polar surfaces. The oppositely charged ions produced positively charged Zn^{2+} $(0\,0\,0\,1)$ and negatively charged O_2^{2-} $(0\,0\,0\,\bar{1})$ polar surface. Different surface termination corresponds to different polarity of the crystal and may lead to different properties. Thus, the large polar surface is generally energetically unfavorable and exhibit massive reconstruction. The anisotropic growth of crystal structure is usually caused by a large difference in

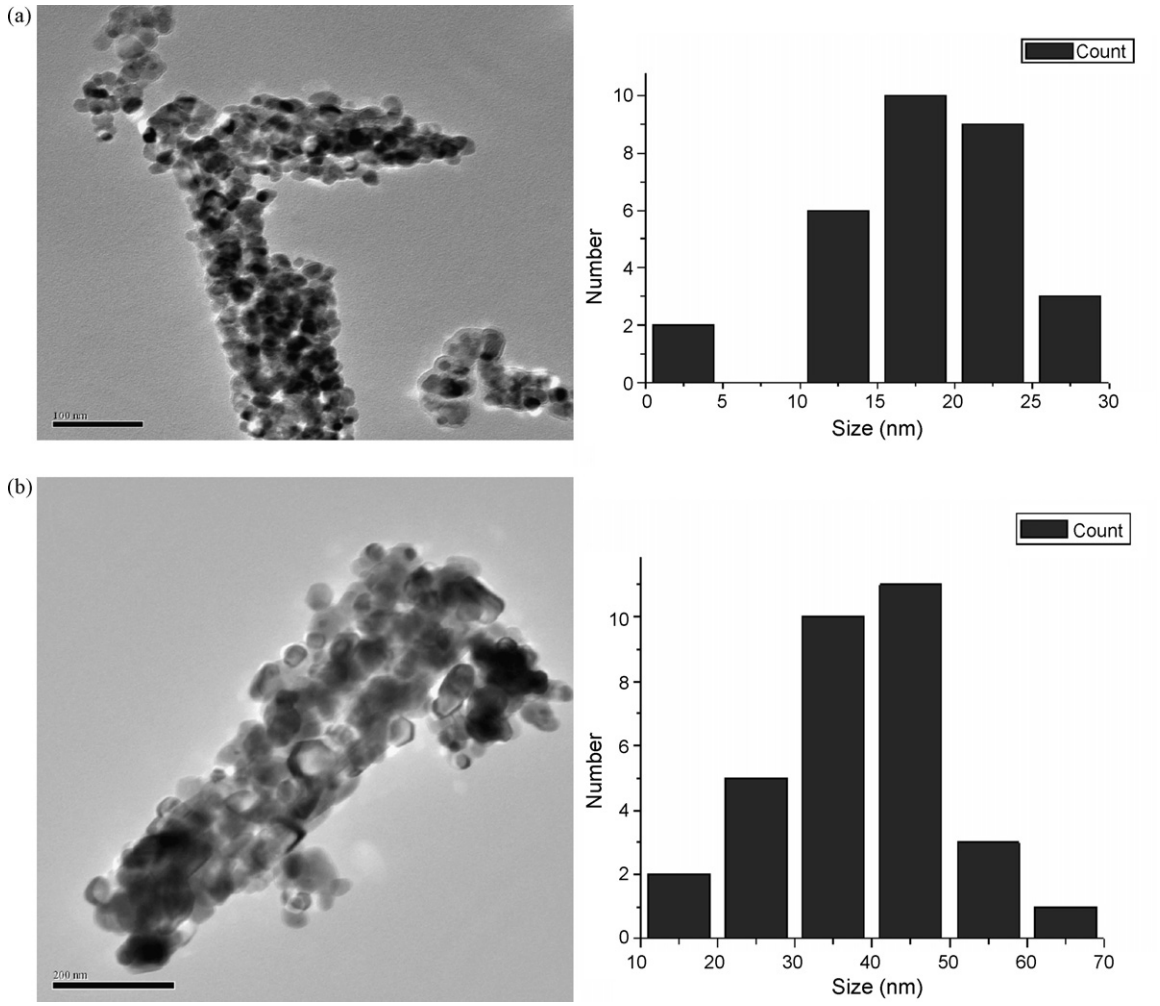

Fig. 5. HR-TEM image of ZnO nanobundles and particle histogram at various times (a) 20 min and (b) 12 h.

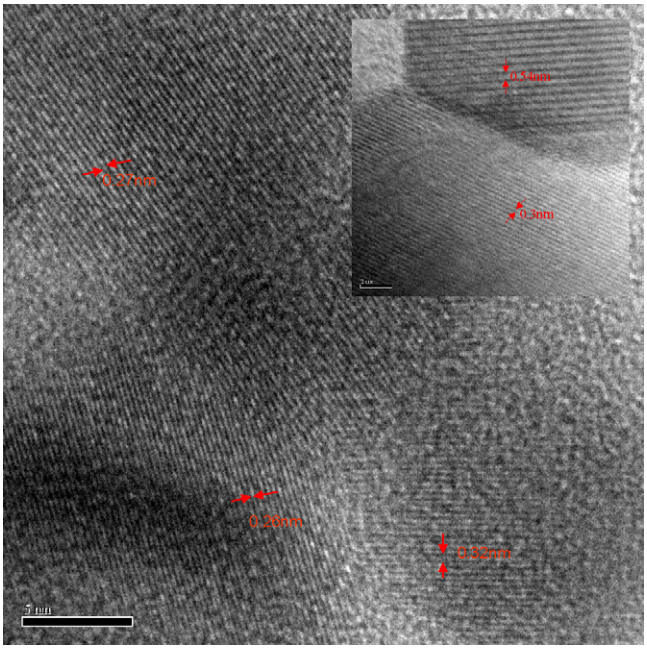

Fig. 6. HR-TEM lattice fringes of as-synthesized ZnO bundles at 20 min [insert image after 12 h].

surface energy between the crystallographic planes. Owing to the anisotropic property of wurtzite ZnO, the resulting uniform ZnO nanoparticles experienced an imperfect-oriented attachment process to lower the system energy, which led to the formation of nanobundles-aggregations. With sufficient energy provided by thermal system, the adjacent nanoparticle piled up and fused each other to further minimize the energy. Similar mechanism is also reported by Zhang et al. in ZnO wire

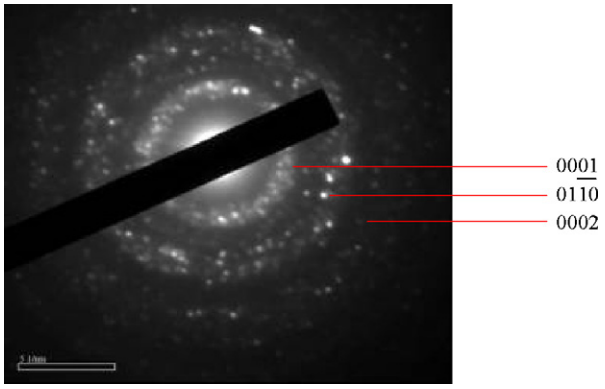

Fig. 7. SAED pattern of ZnO nanobundles.

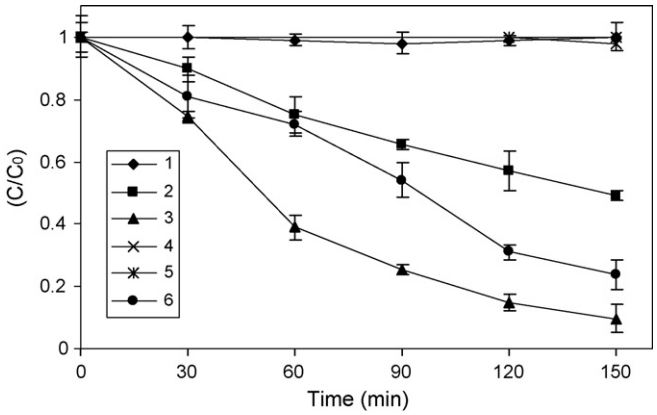

Fig. 8. 2-EEA degradation by various processes. [2-EEA] = 1 g/l, [ZnO] = 2 g/l, pH 3.0 ± 0.1, temperature = 25 °C, and applied ozone dosage = 18.4 mg/l-min. (1) Adsorption process, (2) ozonation process, (3) catalytic ozonation process, (4) ozonation TOC removal process, (5) catalytic ozonation TOC removal process, and (6) with *t*-butanol process.

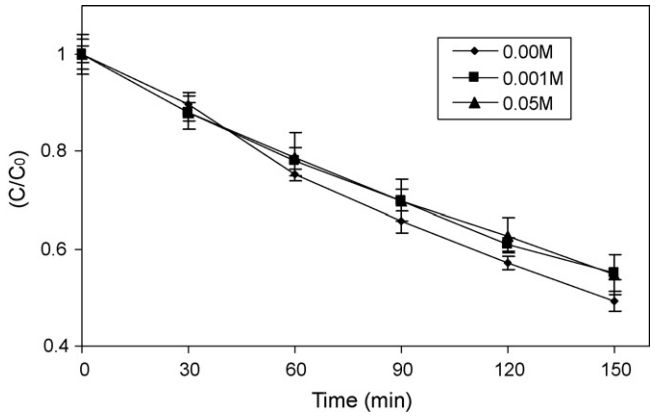

Fig. 9. Effect of *t*-BuOH on the degradation of 2-EEA. [2-EEA] = 1 g/l, pH 3.0 ± 0.1, temperature = 25 °C, and applied ozone dosage = 18.4 mg/l min.

formation [30]. In conclusion, nanobundle formation due to crystallographically specific aggregation based on imperfect-oriented attachment of individual nanoparticles leads to the formation of multi-facetted crystallites with irregular surfaces. Nanobundles are fabricated by a very simple procedure and can be prepared in kilogram scale in low cost.

3.4. Catalytic ozonation using ZnO nanobundles

The catalytic ozonation experiments were carried out in the presence of ZnO at pH 3 using 2-EEA as a model pollutant in batch reactor and the results are shown in Fig. 8. Adsorption experiments showed that 2-EEA is not adsorbed on ZnO surface even after 60 min of contact time. Similar adsorption results were also reported by Jung and Choi on nanosized ZnO catalyst [19]. Ozonation causes 50.7% of 2-EEA decomposition at 150 min and 8% of TOC removal at 600 min while in the presence of ZnO causes 90.4% decomposition and 17.5% of TOC removal at the same time period, which indicates that ZnO is an effective catalyst incorporating with ozonation process. Presence of ZnO nanobundles in ozonation process could enhance 39.7% of 2-EEA decomposition and 9.5% of TOC removal. The enhancement of removal rate in the presence of ZnO bundles is due to generation of hydroxyl radical, which is confirmed in our experiments. A separate experiment has been studied in the presence of 0.025 M *t*-butanol (hydroxyl radical scavenger) and the results are also presented in Fig. 8. Obviously, about 14% of the decomposition rate decreases in the presence of *t*-butanol due to scavenging of hydroxyl radicals generated in the reaction. 2-EEA decomposition is more pronounced than TOC removal. As experienced with the TOC measurements, the mineralization of 2-EEA (1 g/l) is not complete even prolonging reaction time. As observed from the HPLC concentration measurements, the 2-EEA degradation produces a number of intermediate compounds and the removal of these intermediates took longer time. ZnO nanobundles showed a great catalytic effect on the decomposition of 2-EEA in the ozonation process.

3.5. 2-EEA degradation in the presence of radical scavenger and ozone

The oxidizing ability of ozone towards 2-EEA was tested in the presence of radical scavenger without the addition of catalysts at 1 g/l of 2-EEA at 25 °C, and pH 3. In order to test the possible generation of hydroxyl radicals in solution at pH 3, the reaction has been studied in the presence of *t*-butanol (0.001–0.5 mol/l), a compound that reacts very slowly with ozone ($k_D = 0.03\ M^{-1}\ S^{-1}$) [31] but its ability to easily react with hydroxyl radicals ($k_{OH} = 5 \times 10^8\ M^{-1}\ S^{-1}$) is widely known [32]. Therefore, in the presence of *t*-butanol the ozonation process has substantially avoided the reactivity of free radicals towards our target organics. Fig. 9 depicts 2-EEA (1 g/l) degradation at different initial concentrations of *t*-butanol at pH 3 as a function of ozonation time. It is apparent that 2-EEA degradation was not be retarded appreciably in the presence of *t*-butanol, which shows that 2-EEA is mainly oxidized by direct molecular ozone. In conclusion, addition of *t*-butanol does not affect the removal rate.

3.6. Determination of direct reaction constant (k_D)

As discussed above that the addition of *t*-butanol could not affect reaction rate, the direct reaction constant (k_D) of 2-EEA is deduced from the experiments performed at pH 3 without the addition of radical scavenger. Second order rate constant for 2-EEA was determined under conditions where the organic pollutant was excess. Due to the analytical limitation for low concentration measurements of 2-EEA, the decrease of dissolved ozone concentration was monitored instead of the disappearance of the 2-EEA compound [33,34]. The indigo method was applied to monitor the ozone disappearance. In this experiment, the reactor was filled with 500 ml of 4.8×10^{-4} M aqueous ozone solution and 0.0077 M of 2-EEA solution was then injected and the study was commenced. As usual, direct reactions between ozone and organic molecules are described as a bimolecular reaction. The reaction rate is expressed as first order with respect to dissolved ozone concentration [O_3] and first order with respect to the organic compound [S] [35]. The kinetics was determined by the following concentrations of

these compounds as a function of the reaction time.

$$\frac{dC_{O_3}}{dt} = k_D C_{o_3} C_{2-EEA} \quad (1)$$

Integrating Eq. (1) gives

$$\ln\left[\frac{C_{(O_3)t}}{C_{(O_3)0}}\right] = k_D C_{2-EEA} t = k_{obs} t \quad (2)$$

where C_{O_3} = dissolved ozone concentration (mole/L), $C_{2\text{-}EEA}$ = concentration of 2-EEA (mole/L), k_D = direct reaction constant (mole^{-1} s^{-1}), and k_{obs} = apparent rate constant (s^{-1}). Thus, in Fig. 10, it can be seen that when $-\ln[C_{(O_3)t}/C_{(O_3)0}]$ is plotted against time, the data fit a straight line with a regression coefficient of 0.997. From the figure, it can be deduced that the value of k_{obs} is 0.0052 s^{-1}, and, therefore, the value of k_D is 0.675 M^{-1} S^{-1}. Similar low rate constant values (k_D) were reported in the literature [33]. This reaction rate constant implies that ozone is not a potential oxidizing agent for the direct degradation of 2-EEA by ozone molecule, indicating that the 2-EEA oxidation by hydroxyl radicals is thus necessitated for obtaining better removal ability and efficiency.

3.7. Effect of catalyst loading

As we discussed earlier in catalytic ozonation process, the enhancement of removal rate is due to the generation of hydroxyl radicals by ZnO catalyzed ozone decomposition. Because it would be expected that more radical generation at higher catalyst dosage, the influence of catalyst dosage on the removal rate of 2-EEA has been analyzed. Thus, in order to avoid the use of excess catalyst it is necessary to find out the optimum loading dose for the efficient application. Several authors have investigated the reaction rate as a function of catalyst loading in catalytic ozonation process using various catalysts [17,19,36,37]. The effect of catalyst loading on the degradation of 2-EEA was carried out from 0.2 to 3 g/l of the catalyst at 1 g/l of 2-EEA initial concentration and at pH 3.0. Fig. 11 shows the effect of various catalyst dosages on the removal rate at different reaction periods. It seems that the

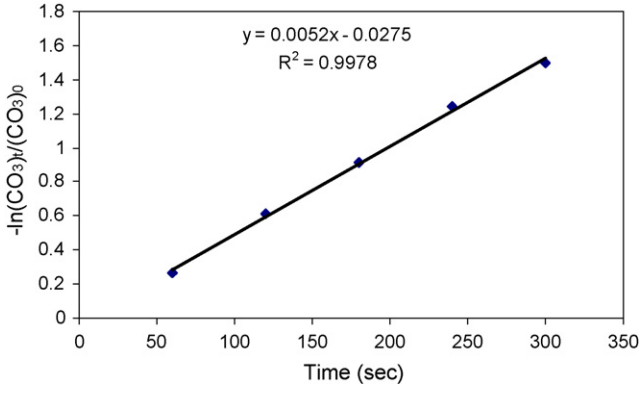

Fig. 10. Determination of direct reaction constant (k_D) of 2-EEA. [2-EEA] = 0.0077 M, $[O_3]_0 = 4.8 \times 10^{-4}$ M, pH 3.0 ± 0.1, and temperature = 25 °C.

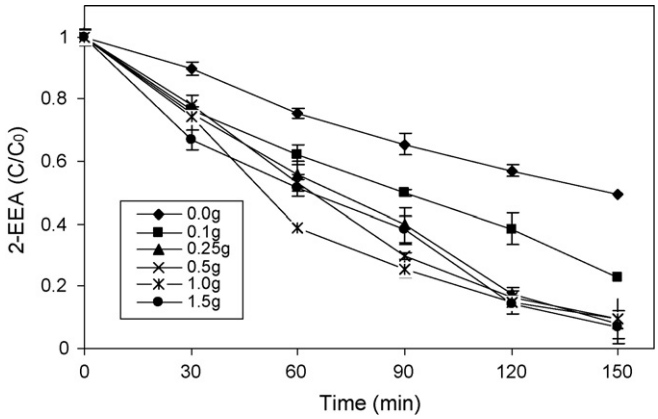

Fig. 11. Effect of catalyst dosage on the decomposition of 2-EEA. [2-EEA] = 1 g/l, pH 3.0 ± 0.1, temperature = 25 °C, and applied ozone dosage = 18.4 mg/l min.

catalyst dose exerted a positive influence on 2-EEA decomposition in catalytic ozonation process. However, the increase of catalyst dose from 2 to 3 g/l did not increase the degradation rate appreciably. About 38%, 44%, 47%, 61% and 48.5% of decomposition was observed after 60 min at 0.2, 0.5, 1, 2, 3 g/l of ZnO, respectively. However, at the end of reaction periods (150 min) the removal rates are 76.9%, 92%, 90.3%, 90.4% and 93%. Although, a slight difference in the removal rate was observed in initial reaction periods, the removal rate was almost similar after 120 min of reaction time above 0.5 g/l of catalyst loading. Similar trends were also reported by Carbajo et al. in phenolic wastewaters degradation using perovskite-type catalysts and concluded that the degradation efficiency at the end of reaction period was independent of catalyst dosage [36]. Several authors reported controversial to the reference above in catalytic ozonation experiments. For example, Park et al. reported that the *p*CBA degradation rate linearly depends on goethite catalyst concentration from 2 to 15 g/l [38]. Jung and Choi also noted similar results in *p*CBA degradation using nanosize ZnO as catalysts range from 26.9 to 108.2 mg/l [19]. In summary, the removal efficiency is increased when the catalyst loading increases from 0.2 to 3 g/l. However, 2 g/l of ZnO catalyst is found to be optimum dosage. In all other experiments, 2 g/l of catalysts dosage was used.

3.8. Catalytic reusability and recyclability of nanobundles

Any catalyst after finishing their regular tasks in chemical investigation and chemistry industry is expected to be reclaimed and recycled by proper and simple treatment. In fact, deactivation of the catalyst is a frequently encountered phenomenon. Due to the oxidizing characteristics of ozone and hydroxyl radical, it may chemically interact with catalysts and can alter the catalytic properties. For example, in our previous studies, although we found that ozone decomposition on sludge catalysts could alter the surface characteristics of sludge catalysts up to four cycles, its ozone decomposition ability of the catalysts was not affected [39]. Qu et al. have found that the activated carbon fiber losses its phenol adsorption ability in catalytic ozonation process at repeated use. However, it did not

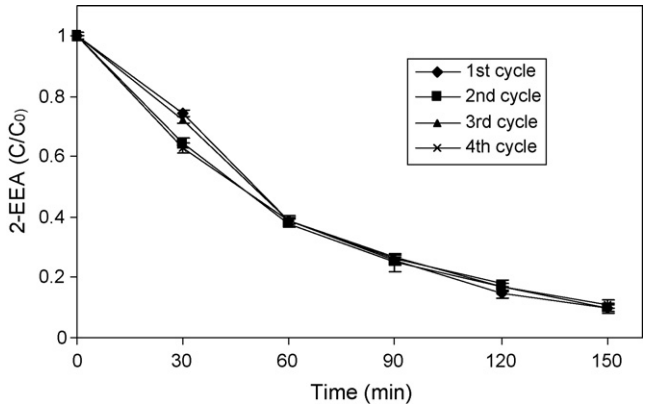

Fig. 12. Effect of catalytic reusability on the decomposition of 2-EEA. [2-EEA] = 1 g/l, [ZnO] = 2 g/l, pH 3.0 ± 0.1, temperature = 25 °C, and applied ozone dosage = 18.4 mg/l min.

lose its catalytic activity up to four consecutive cycles [17]. Carbajo et al. found catalytic deactivation in $LaTi_{0.15}Cu_{0.85}O_3$ catalyst in catalytic ozonation process due to copper leaching up to four cycles and a significant deterioration was observed in the mineralization efficiency [36]. Since the catalytic stability and reusability are important factors in catalyzed reactions, it is necessary to study the stability of the used catalyst. If the stability is poor or deactivation of the catalyst is severe, the catalyst will be useless in a practical industrial application. The entire catalytic reusability test has been investigated under identical reaction conditions. At the end of the oxidation process (150 min), the catalyst can be easily removed from the reactor and then be washed gently with large amount of deionized water (18.2 M Ω) and 25 ml of methanol. The washed catalysts were dried in atmospheric condition and in an oven at 100 °C for 30 min to remove molecular water present on the surface of the catalysts. Fig. 12 shows 2-EEA decomposition results of the recovered catalysts. After 60 min, about 59% decomposition was observed in all cycles. This result implies that successive use of the catalysts does not influence catalytic activity of ZnO bundles. In conclusion, there is no obvious decrease in the 2-EEA decomposition efficiency in successive usages. These results indicate that the catalyst has an excellent long-term stability. The excellent stability of the catalytic activity could be attributed to the stable structure of the catalyst, which is also confirmed by the XRD and SEM measurements (not shown in Figures). The catalytic recyclability of ZnO nanobundles has been studied and compared with other commercially available metal oxide catalysts such as ZnO and TiO_2-P25 nanocatalysts. About 0.5 g of all these three catalysts were suspended in 500 ml of Milli q-Plus water and magnetically stirred for 5 min and the separation was noted after 5 min as shown in the Fig. 13. Obviously, ZnO nanobundles (A) are quite easily separated in a short time when compared to commercial ZnO (B) and TiO_2-P25 (C) nanocatalysts, which shows that the ZnO nanobundles are easily recyclable catalysts. Similar observation was also reported in the literature in anatase TiO_2 nanoparticles immobilized on ZnO tetrapods [40]. In conclusion, ZnO nanobundles are highly efficient and easily recyclable catalyst.

Fig. 13. Catalytic recyclability of ZnO nanobundles. [A] = ZnO nanobundles, [B] = ZnO nanoparticle, and [C] = TiO_2-P25 nanoparticle.

4. Conclusions

A new self-assembly of ZnO nanobundles building block has been successfully fabricated and used in catalytic ozonation process. The as-synthesized ZnO nanobundles were characterized using XRD, FESEM, HR-TEM, and thermal analysis. The formation of ZnO nanobundles and its mechanism has been discussed. The catalytic activity of ZnO nanobundle was investigated in catalytic ozonation process using 2-EEA as a target pollutant. The adsorption studies showed that 2-EEA was not adsorbed on the catalyst and addition of ZnO nanobundles strongly enhances 2-EEA removal rate in ozonation process. Almost, complete degradation is observed in 180 min, however, a partial mineralization is noted. The enhancement of removal rate in catalytic ozonation process is due to the generation of hydroxyl radicals which accelerate the decomposition rate. The direct reaction rate constant (k_D) value showed that the ozone alone is not a potential oxidizing agent. 2 g/l of catalysts dosage was found to be optimum dosage for efficient removal. The catalytic reusability was investigated up to four successive cycles and found that the catalytic efficiency was not decreased appreciably. In conclusion, ZnO nanobundles are efficient and easily recyclable catalysts in catalytic ozonation process.

Acknowledgement

The authors wish to acknowledge the financial support from National Science Council in Taiwan under the contract number of NSC-95-2221-E-035-060.

References

[1] X.Y. Kong, Y. Ding, R. Yang, Z.L. Wang, Science 303 (2004) 1348.
[2] B. Liu, H.C. Zeng, J. Am. Chem. Soc. 125 (2003) 4430.
[3] Y. Dai, Y. Zhang, Y.Q. Bai, Z.L. Wang, Chem. Phys. Lett. 375 (2003) 96.
[4] S. Kar, A. Dev, S. Chaudhuri, J. Phys. Chem. 110 (2006) 17848.
[5] G. Shen, Y. Bando, B. Liu, D. Golberg, C.-J. Lee, Adv. Funct. Mater. 16 (2006) 410.

[6] J.Y. Lao, J.Y. Huang, D.Z. Wang, Z.F. Ren, Nano Lett. 3 (2) (2003) 235.
[7] R.L. Penn, J.F. Banfield, Science 281 (1998) 969.
[8] R.L. Penn, J.F. Banfield, Geochim. Cosmochim. Acta 63 (1999) 1549.
[9] J.F. Banfield, S.A. Welch, H. Zhang, T.T. Ebert, R.L. Penn, Science 289 (2000) 751.
[10] C. Pacholski, A. Kornowski, H. Weller, Angew. Chem. Int. Ed. 41 (2002) 1188.
[11] D. Dollimore, D. Nicholson, J. Chem. Soc. 178 (1964) 908.
[12] D. Dollimore, J. Dollimore, D. Nicholson, J. Chem. Soc. 308 (1965) 2132.
[13] L. Guo, Y. Ji, H. Xu, Z. Wu, P. Simon, J. Mater. Chem. 13 (2003) 754.
[14] Z. Zhang, J. Mu, J. Colloid Interface Sci. 307 (2007) 79.
[15] K.B. Hordern, U.R. Stanislawiak, J. Swietlik, J. Nawrocki, Appl. Catal. B: Environ. 62 (2005) 345.
[16] R. Andreozzi, V. Caprio, A. Insola, R. Marotta, V. Tufano, Ind. Eng. Chem. Res. 36 (1997) 4774.
[17] Y. Yang, J. Ma, Q. Qin, X. Zhai, J. Mol. Catal. A: Chem. 267 (2007) 41.
[18] M. Sánchez-Polo, J. Rivera-Utrilla, Appl. Catal. B: Environ. 67 (2006) 113.
[19] H. Jung, H. Choi, Appl. Catal. B: Environ. 66 (2006) 288.
[20] W.-J. Huang, G.-C. Fang, C.-C. Wang, Colloids Surf. A: Physico. Chem. Eng. Asp. 260 (2005) 45.
[21] J.J. Wu, C.C. Wu, H.W. Ma, C.C. Chang, Chemosphere 54 (2004) 997.
[22] H. Bader, J. Hoigne, Water Res. 15 (1981) 449.
[23] L. Yang, G. Wang, C. Tang, H. Wang, L. Zhang, Chem. Phys. Lett. 409 (2005) 337.
[24] H.G. Yang, H.C. Zeng, J. Phys. Chem. B 108 (2004) 3492.
[25] Y. Yin, R.M. Rioux, C.K. Erdonmez, S. Hughes, G.A. Somorjai, A.P. Alivisatos, Science 304 (2004) 711.
[26] S. Park, J.-H. Lim, S.-W. Chung, C.A. Mirkin, Science 303 (2004) 348.
[27] H. Zhang, J.F. Banfield, Nano Lett. 4 (2004) 713.
[28] Z. Tang, N.A. Kotov, M. Giersig, Science 297 (2002) 237.
[29] C. Ribeiro, E.J.H. Lee, T.R. Giraldi, J.A. Varella, E. Longo, E.R. Leite, J. Phys. Chem. B 108 (2004) 15612.
[30] D.-F. Zhang, L.-D. Sun, J.-L. Yin, C.-H. Yan, R.-M. Wang, J. Phys. Chem. B 109 (2005) 8786.
[31] J. Hoigne, H. Bader, Water Res. 17 (1983) 173.
[32] J. Hoigne, Water Sci. Technol. 35 (1997) 1.
[33] J.L. Acero, S.B. Haderlein, T.C. Schmidt, M.J.-F. Suter, U.V. Gunten, Environ. Sci. Technol. 35 (2001) 4252.
[34] M.M. Huber, S. Canonica, G.-Y. Park, U.V. Gunten, Environ. Sci. Technol. 37 (2003) 1016.
[35] J. Hoigne, J. Hrubec (Eds.), Chemistry of aqueous ozone and transformation of pollutants by ozonation and advanced oxidation processes, vol. 5, Springer-Verlag, Berlin, Hedelberg, 1998, pp. 83–141 (part C).
[36] M. Carbajo, F.J. Beltrán, O. Gimeno, B. Acedo, F.J. Rivas, Appl. Catal. B: Environ. 74 (2007) 203.
[37] F.J. Rivas, M. Carbajo, F.J. Beltrán, B. Acedo, O. Gimeno, Appl. Catal. B: Environ. 62 (2006) 93.
[38] J.S. Park, H. Choi, J. Choi, Water Res. 38 (2004) 2285.
[39] M. Muruganandham, S.H. Chen, J.J. Wu, Catal. Commun. 8 (2007) 1609.
[40] Q. Zhang, W. Fan, L. Gao, Appl. Catal. B: Environ. 76 (2007) 168.